RSC Advances

PAPER

View Article Online
View Journal | View Issue

Check for updates

Cite this: *RSC Adv.*, 2024, **14**, 2048

# Cellulose nanocrystals extracted from rice husk using the formic/peroxyformic acid process: isolation and structural characterization†

An Nang Vu, *[ab] Long Hoang Nguyen,[ab] Ha-Chi V. Tran,[ab] Kimio Yoshimura,[d] Tap Duy Tran,[ab] Hieu Van Le [abc] and Ngoc-Uyen T. Nguyen [ab]

Received 3rd October 2023
Accepted 22nd December 2023

DOI: 10.1039/d3ra06724f

rsc.li/rsc-advances

Cellulose derived from biomass is a renewable resource with numerous applications. Using formic/peroxyformic acid at atmospheric pressure, cellulose nanocrystals (CNC) were isolated from rice husk (RH) in this study. This method was an excellent way to get rid of lignin and hemicelluloses from RH. The cellulose was subsequently acid hydrolyzed by $H_2SO_4$ (64%) for 30 minutes at 45 °C. The chemical and microstructure analysis showed that the lignin and hemicellulose contents of raw RH had been eliminated, and the crystallinity content of CNC was 67.16%. According to transmission electron microscopy (TEM) morphological analysis, CNC measured 19 ± 3.3 nm in diameter, 195 ± 24 nm in length, and 10.2 ± 6.8 in aspect ratio. The thermal stability of RH and CNC was also investigated using thermogravimetric analysis (TGA). These encouraging findings demonstrated the potential for reusing RH agricultural waste to create CNC and include nanocomposites as a reinforcing material.

## 1. Introduction

This century's "bioeconomy" paradigm promotes using renewable materials over non-renewables for economic success and environmental sustainability.[1] With an annual production of approximately $7.50 \times 10^{10}$ tons, cellulose biopolymer is one of the most abundant materials. Cellulose comprises repeated D-glucopyranosyl units connected by β-(1-4)-glycoside bonds.[2] Due to the interaction of high molecular weight polymer chains, both crystalline and amorphous regions are presented in cellulose. Crystalline particles called cellulose nanocrystals (CNC) are created when amorphous cellulose is hydrolyzed with acid.[3] CNC has several notable characteristics, including its low cost, lack of toxicity, exceptional thermal stability, optical transparency, and biodegradability.[4] CNC can be extracted from various biomasses and widely used as a polymer composite reinforcement because of its excellent thermal and mechanical properties, including high elasticity modulus (about 150 GPa),[5] ultralightweight nature (1.6 g $cm^{-3}$),[6] and large specific surface area (hundreds of $m^2$ $g^{-1}$).[7] CNC improves several biodegradable polymers' physicochemical, thermal, and insulating characteristics, making them acceptable for many applications.[8] Furthermore, CNC can be utilized in the production of barrier films,[9] shape-memory polymers,[10] bio-nanocomposites,[11] drug-delivery materials,[12] photonic crystals,[13] biomedical devices,[13] filaments,[14] aerogels,[15] hydrogels,[16] fuel cells,[17] and three-dimensional (3D) printing,[18] as well as for wastewater treatment,[19] agricultural product production,[20] adsorption,[21] and cultural heritage materials.[22] The surface chemistry of cellulose derivatives can be altered for numerous additional applications.[23]

Current research has focused on extracting CNC from agricultural byproducts using chemical, mechanical, and enzymatic approaches.[24,25] Due to the inherent drawbacks associated with mechanical techniques, such as their time-consuming nature and the need for high pressure and kinetic energy, as well as the limitations of enzymatic methods, which are often tedious and reliant on the capabilities of microorganisms, chemical methods have emerged as the favored choice for achieving more efficient cellulose isolation. These chemical methods can be employed independently or with mechanical or enzymatic approaches. Several studies have used diverse raw material sources, including sugarcane bagasse,[26] coconut fiber,[27] rice straw,[28] banana plant pseudostems,[29] and tea leaf waste.[30] The rice husk (RH) is a natural fiber that develops around the rice kernel and is removed during rice production. Prior research focused on the high-temperature treatment of RH to extract silica[31] or the surface treatment of RH for application as a reinforcing component in lightweight composites.[32]

[a]Faculty of Materials Science and Technology, University of Science, VNU-HCM, 700000, Vietnam. E-mail: vnan@hcmus.edu.vn

[b]Vietnam National University, Ho Chi Minh City, 700000, Vietnam

[c]Laboratory of Multifunctional Materials, University of Science, VNU-HCM, 700000, Vietnam

[d]Department of Advanced Functional Materials Research, Takasaki Advanced Radiation Research Institute, National Institutes for Quantum Science and Technology (QST), Takasaki, Gunma 370-1292, Japan

† Electronic supplementary information (ESI) available. See DOI: https://doi.org/10.1039/d3sc06206f

Open Access Article. Published on 09 January 2024. Downloaded on 1/19/2026 7:03:55 PM. This article is licensed under a Creative Commons Attribution-NonCommercial 3.0 Unported Licence.



© 2024 The Author(s). Published by the Royal Society of Chemistry

Open Access Article. Published on 09 January 2024. Downloaded on 1/19/2026 7:03:55 PM.
This article is licensed under a Creative Commons Attribution-NonCommercial 3.0 Unported Licence.

For the past two decades, in Vietnam, the surface of RH has been treated using various chemical methods as a heavy metal adsorption material or a filler in the fabrication of composite materials.[33] The most recent is using RH as a raw material source for thermally treating silica or activated charcoal. Vietnam is an agricultural country whose principal food source is rice. In 2016, Vietnam's rice production topped 42 million tons, with rice residue accounting for 20% of total production. Most RHs are torched or discarded. When RHs are burned, an enormous amount of ash is formed during carbon metabolism. It exists as thin, light granules that might aggravate human respiratory disorders.[32] Furthermore, bacteria decomposing the debris will generate methane gas, which hurts the environment. These variables make processing this waste more difficult. Therefore, more research is needed on utilizing this abundant raw material source.

RH has four essential parts that make up its structure: cellulose (25–35%), hemicellulose (18–21%), lignin (18–21%), and silica (15–17%). The rest comprises soluble chemicals and water (7–15%).[34] As a result, research incorporating rice chaff as a raw material source for synthesizing CNC is in high demand. This research aims to isolate cellulose from Vietnamese RH and hydrolyze CNC for reinforced-phase applications in composite materials. The isolation of cellulose was achieved *via* the formic/peroxyformic acid method, comprising three principal stages: formic acid treatment (HCOOH), peroxyformic acid treatment (PFA, a solution of HCOOH and $H_2O_2$), and bleaching with a solution of NaOH and $H_2O_2$. As far as the authors know, this is the first study to describe the delignification of lignocellulosic biomass and the extraction of cellulose fibers from RH using a pre-treated process involving formic/peroxyformic acid. For decontaminating biomass, sodium chlorite ($NaClO_2$), sodium hypochlorite (NaClO), chlorine dioxide ($ClO_2$), chlorine ($Cl_2$), and hydrogen peroxide ($H_2O_2$) were utilized.[35–37] Although less effective than alternative bleaching agents, $H_2O_2$ is still regarded as a greener alternative to chlorinated solutions.[38] This investigation's unconventional aspect is utilizing an oxidant ($H_2O_2$) and alkali (NaOH) solution to extract cellulose fibers, depolymerize lignin and remove hemicellulose. Under specific conditions, NaOH, a potent alkaline chemical, can eliminate hemicellulose and lignin.[39] Bleaching with an alkaline hydrogen peroxide solution (pH 8–12) aims to enhance the whiteness of the cellulose by dissolving any remaining lignin and hemicellulose. The hydroperoxide anion ($HOO^-$) in the alkaline media oxidized the lignin structure, forming more cellulose-rich fibers and a lighter color.[40]

Furthermore, the literature contains several noteworthy reports concerning biomass pre-treatment, which encompass acidic and alkaline treatment, pulping, and bleaching.[41,42] Implementing acidic or alkaline pre-treatment methods during cellulose isolation increases costs for corrosion-resistant materials and post-processing technologies required to neutralize or eliminate corrosive chemicals. As most inorganic acids are highly corrosive and difficult to recover, conventional inorganic acid pre-treatment violates the rules of sustainable and green chemistry.[43] Using vacuum distillation or recrystallization, organic acids can be easily recycled and are less corrosive than inorganic acids.[24,44] Another innovation of this study is incorporating formic acid, the simplest carboxylic acid characterized by its low boiling point (100.8 °C)[45] and relatively strong acidity. This acid was utilized to dissolve hemicellulose partially, cause it to swell, and facilitate lignin migration to the RH surface. As a result, the bleaching stage for cellulose isolation was significantly enhanced in efficiency.

## 2. Experimental

The RHs originated in the Cu Chi rice-growing region of Ho Chi Minh City. After collection, they were rinsed with water, sun-dried, and ground into a fine powder. Sodium hydroxide (NaOH, 96%), hydrogen peroxide ($H_2O_2$, 30%), formic acid (HCOOH, 90%), and sulfuric acid ($H_2SO_4$, 98%) originate from Xilong Scientific Co. China. All are commercial chemicals and were used directly.

### 2.1. Preparation of cellulose

The sequential process of cellulose isolation from RH involved three primary steps: HCOOH acid treatment, peroxyformic acid (PFA) treatment, and bleaching using a NaOH/$H_2O_2$ mixture. Initially, the RH powder was immersed in distilled water, followed by boiling at 100 °C for 2 hours to eliminate impurities. Subsequently, the mixture underwent filtration and desiccation at 70 °C for 8 hours. The homogenous blending of RH powder was treated with a 90% HCOOH solution at a ratio of 1 : 15 (RH powder to 90% HCOOH acid volume) at 80 °C. After 2 hours, the sludge was filtered, rinsed with hot water, and desiccated at 80 °C for 6 hours before PFA treatment. A solution of PFA, comprising 90% HCOOH, 4% $H_2O_2$, and 6% $H_2O$, was added to RH powder. For 2 hours, the PFA treatment was kept at 80 °C. The filtration method was used to separate the solid product. The substance was carefully washed with distilled water until the pH reached 6–7. After drying for 12 hours at 80 °C, the solid product was bleached with a NaOH/$H_2O_2$ mixture. Using a 1 M NaOH solution, the pH of the suspension was carefully adjusted to 11. After that, 30% $H_2O_2$, equal to 40% of the solid mass in the rest, was slowly added. The mixture was then mixed for an hour at 80 °C.

### 2.2. Production of cellulose nanocrystals (CNC)

To make CNC, RH cellulose was broken down with a 64% sulfuric acid solution (1 : 20 ratio of solid mass to acid volume) at 45 °C for 30 minutes. The mixture was carefully put into a container with 1000 mL of distilled water to finish the process. The solution was diluted with water until pH 7 was obtained. The resultant mixture was centrifuged at 4000 rpm for 10 minutes, twice with distilled water and thrice with ethanol. After drying out at 80 °C until the mass stayed the same, a sample of white powder was taken as the result. CNC yield was determined using RH starting weight.[46]

### 2.3. Characterizations

**2.3.1. Fourier transform infrared spectroscopy (FT-IR).** The chemical structure of unprocessed, acid-treated, PFA-treated,

Open Access Article. Published on 09 January 2024. Downloaded on 1/19/2026 7:03:55 PM. This article is licensed under a Creative Commons Attribution-NonCommercial 3.0 Unported Licence.

bleached, and CNC extracted from RH was investigated using FT-IR. Samples were placed on KBr discs, and a Nicolet 6700 spectrometer (M/S Thermo Fisher Scientific Instruments, USA) was used to record spectral signals with an average of 32 scans, 4 $cm^{-1}$ resolution. OMNIC 9.2.86 (Thermo Fisher Scientific, Inc., USA) software was used to smooth the obtained spectra.

**2.3.2. X-ray diffraction (XRD).** XRD was used to reveal the structural modifications of materials at every stage of treatment. XRD (D2 PHASER, Bruker, Germany) spectra with Cu-K$\alpha$ ($\lambda$ = 0.15418 nm), 30 kV, and 10 mA were utilized to calculate the crystal size and crystallinity fraction. The dried samples were put on the quartz base, and scans were taken at a speed of 0.02° $min^{-1}$ over a 2$\theta$ range of 10°–80°. Duplicate XRD analyses were performed on each material. The XRD diffractograms were smoothed and analyzed with Xpert HighScore Plus (PANalytical Technologies Pvt. Ltd, Netherlands) software. The Gauss function in OriginPro 9.0.0 (64 bit) (OriginLab Corporation, USA) was used to fit the curve. The percentage of crystallinity (CrI) was calculated using eqn (1) below based on the areas beneath the crystalline and amorphous peaks after baseline correction.[47]

$$\mathrm{CrI}\ (\%) = A_c/(A_c + A_a) \times 100 \quad (1)$$

where $A_a$ and $A_c$ are the areas under the amorphous and the crystalline peaks, respectively.

Scherrer's eqn (2) was applied to calculate the dimension $D_{hkl}$ of the crystallites parallel to the *hkl* diffracting planes.

$$D_{hkl} = (K \times \lambda)/(\beta_{1/2} \times \cos\theta) \quad (2)$$

where correction factor $K$ is 0.9, $\lambda$, $\theta$, and $\beta_{1/2}$ are the wavelength, the diffraction angle, and the peak width at half maximum intensity, respectively.

**2.3.3. Thermal analysis (TGA).** TGA was used to compare the decomposition characteristics of materials at different stages of treatment. The temperature stability of each sample was measured with a TGA/DTA thermogravimetric analyzer (Mettler Toledo Corporation, Schwarzenbach, Switzerland), and the results were analyzed with STAR software (Version 9.3). Runs were done by putting between 2 and 4 mg of the sample into a 70 μL aluminum cup. Just before the analysis, the cup was crimped, and the instrument automatically poked a hole in it. The investigation was conducted with a steady nitrogen supply of 40 mL $min^{-1}$ to ensure that the weight loss was caused by thermal degradation. The temperature of the sample was ramped at a constant rate of 10 °C $min^{-1}$, and weight loss (TGA) or heat evolved (DTA) was measured against increasing temperature.

**2.3.4. Transmission electron microscopy (TEM).** TEM (JEM-1400 F, JEOL Ltd, Tokyo, Japan) observations were carried out in duplicate at 100 kV accelerating voltage to study the morphology of CNC. Micropipette drops of 1.0 wt% CNC suspension were placed on copper grids, dried at ambient temperature, and examined using TEM.

**2.3.5. Raman spectroscopy analysis.** The Raman spectra were taken with laser Raman microspectroscopy (XploRA Plus, Horiba) at an excited wavelength of 785 nm and a power of 0.5 mW to prevent the laser heating from affecting the Raman shift of the CNC material. The spectrum was obtained by aggregating three separate scans of distinct CNC sample regions. All spectral changes were done with Origin Pro 9.0.0 (OriginLab, USA).

**2.3.6. Solid-state $^{13}$C nuclear magnetic resonance ($^{13}$C-NMR).** Solid-state $^{13}$C-NMR experiments were performed on a Bruker AVANCE 400 spectrometer using cross-polarization, high-power proton decoupling, and magic angle spinning (CP/MAS). $^{13}$C-NMR spectra were obtained at 298 K using a 4 mm probe at 100.13 MHz. The CP contact periods were 2 ms, the repetition duration was 1 s, and the MAS rotation frequency was 12 kHz.

# 3. Results and discussion

## 3.1. Physical appearance of RH at different treatment stages

According to Fig. 1, the color of RH changed from light brown to reddish brown following treatment with acid and PFA and then to a clear white following bleaching because of the elimination of hemicellulose, lignin, and other non-cellulosic substances. RH was subjected to an acidic environment to partially dissolve hemicellulose, wax, and pectin. Rest and lignin swelled in the acidic environment and migrated toward the surface, facilitating the PFA process. The sample color at this stage was a deeper reddish brown than the original because the phenol derivatives found in lignin absorb visible light.

The PFA phase softened the fiber by removing a significant portion of hemicellulose and some lignin due to oxidant $H_2O_2$. Most RH hemicellulose, wax, and pectin have been extracted using acid and PFA processing. However, unlike when the fiber was treated with HCOOH, the lignin stayed outside of it, swelled, and migrated to the exterior of the fiber, giving the fiber a deeper color. Therefore, further bleaching is required to eliminate lignin and obtain purified cellulose. Cellulose fiber is a semi-crystalline material made up of solid and amorphous parts.

Consequently, the final step involves acid hydrolysis, in which the acid targets prioritize attacking amorphous regions while avoiding crystalline areas. The primary function of acids is to liberate hydronium ions ($H^+$) to degrade the glycoside and ether bonds in the cellulose molecular chain of the amorphous region. After acid hydrolysis, colloidal suspensions of CNC were homogeneous and stable.

## 3.2. FTIR

The chemical composition of materials undergoing various chemical treatments has been directly determined using FTIR spectroscopy. The FTIR spectra of raw, acid-treated, PFA-treated, bleached, and acid hydrolysis RH are shown in Fig. 2. The prominent bands found in the FTIR spectra of the various treated RH samples are thoroughly summarized in Table S1.† The peak in the 3440–3450 $cm^{-1}$ range attributed to O–H stretching vibrations of cellulose molecules was seen in all samples. This observation emphasizes the fibers' underlying hydrophilic nature. The C–H bond's asymmetric stretching vibration has a designated frequency range of 2900–

 © 2024 The Author(s). Published by the Royal Society of Chemistry

Open Access Article. Published on 09 January 2024. Downloaded on 1/19/2026 7:03:55 PM.
This article is licensed under a Creative Commons Attribution-NonCommercial 3.0 Unported Licence.

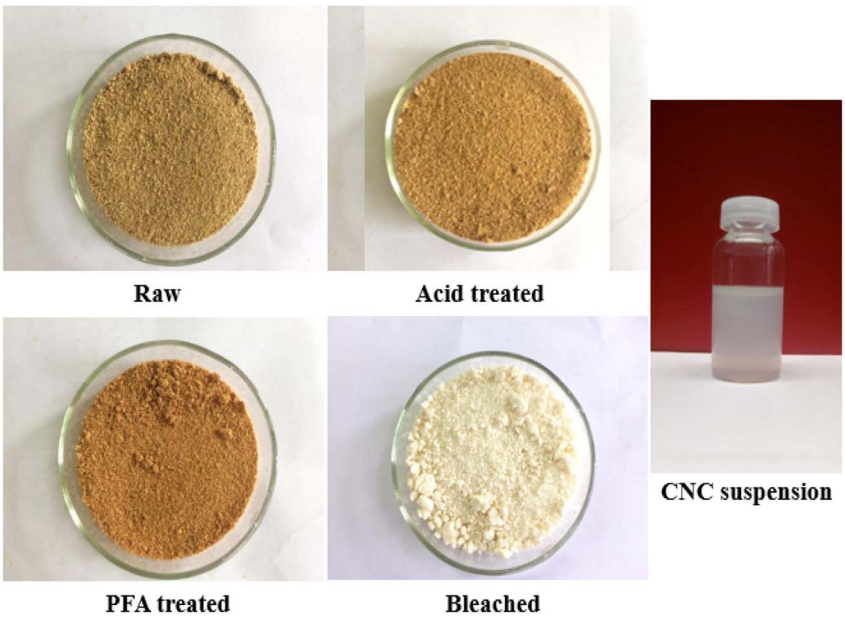


Fig. 1 RH photographs at various phases of chemical treatment and CNC suspension.

2937 $cm^{-1}$.[48] A shoulder at 1740 $cm^{-1}$ in RH spectra revealed acetyl and ester in hemicellulose or carboxylic acid groups in ferulic and *p*-coumaric lignin.[49–51]

The hemicellulose components of RH were dissolved when exposed to HCOOH and PFA acid at 80 °C. The lignin component became flatter and moved closer to the surface. This made the 1740 $cm^{-1}$ peak in the PFA-treated sample more noticeable than in the raw RH sample. This peak disappeared from the spectra of the bleached and acid hydrolysis samples, indicating that the hemicelluloses and lignin in the fibers were extracted chemically. The perceptible alterations in the location and shape of the FTIR peaks demonstrated the observable structural alteration.

The peak found at 1645 $cm^{-1}$ in all spectra can be assigned to the bending vibration of O–H in the adsorbed water on the cellulose structure.[52,53] The typical C–O stretching vibration of lignin and hemicellulose of raw RH was found at 1247 $cm^{-1}$ [51,53] and was absent from the bleached and acid-hydrolyzed samples, indicating the sufficient removal of hemicellulose lignin components during the chemical treatments. The

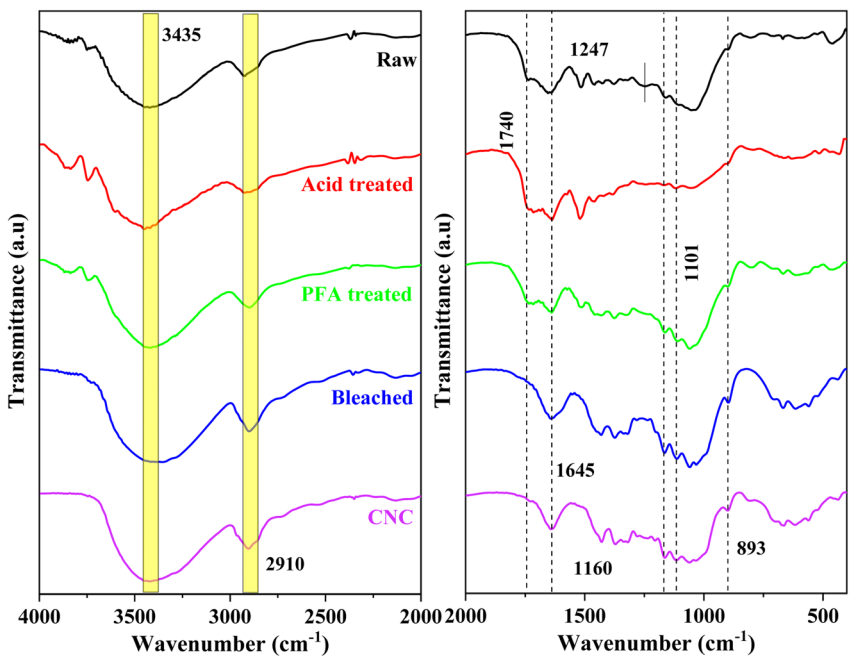


Fig. 2 FTIR spectra of RH at distinct chemical treatment stages and CNC.

Open Access Article. Published on 09 January 2024. Downloaded on 1/19/2026 7:03:55 PM. This article is licensed under a Creative Commons Attribution-NonCommercial 3.0 Unported Licence.

deformation vibration of the C–C bond in the ring and the glycoside ether bond (C–O–C) in the β-1,4-glycosidic bond of cellulose were assigned to at 1160 $cm^{-1}$ and 1101 $cm^{-1}$.[54] The absorption recorded in all 1024–1047 $cm^{-1}$ spectra corresponded to the cellulose component's C–H stretching vibration.[52] The results revealed that the cellulose molecular structure remained unchanged following acid hydrolysis. The spectra's signal at 893 $cm^{-1}$ was linked to the cellulose glucose ring's glycosidic linkages.[55] This peak was more noticeable after bleaching and acid hydrolysis, indicating that the cellulose content had grown due to further extraction steps. The spectral values discovered agreed with the available literature.[55] The FTIR spectra of the bleached and acid hydrolysis samples without contaminants were compared to those of the unprocessed RH based on the discussion and analysis that came before them. For example, the RH peaks at 1740 $cm^{-1}$ and 1247 $cm^{-1}$ were no longer present. According to the findings, lignin and hemicellulose were eliminated using chemical treatment.[56]

### 3.3. XRD

XRD patterns can be utilized to examine the crystalline structure of the untreated and chemically treated cellulose fibers, as illustrated in Fig. 3. All diffractograms showed two peaks, at around 22° and 15°, that corresponded to the crystalline structure of cellulose I.[57] Hydroxyl groups in cellulose can form intermolecular and intramolecular bonds, leading to cellulose crystalline structures.[58] This bonding prevents the movement of cellulose chains and makes them align tightly and orderly, leading to a propensity for crystallinity. In unprocessed fiber, these crystalline regions are surrounded by amorphous parts like hemicelluloses, lignin, and pectin, making the fiber less crystalline. The pattern indicated that the crystallinity improved due to the effective removal of non-crystalline components using a series of chemical treatments.

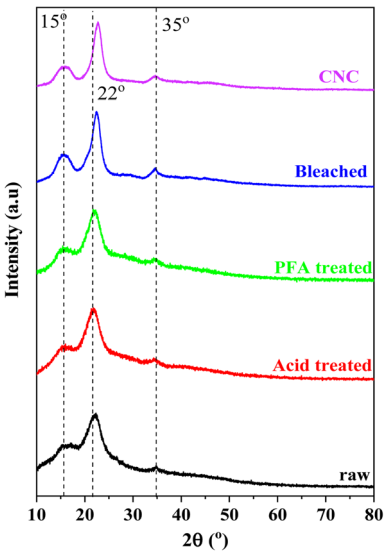


Fig. 3 XRD pattern of RH at distinct treatment stages.

Table 1 CrI and crystalline domain size of RH at different stages of treatment

| RH stage | CrI (%) | Crystalline domain size (nm) |
|---|---|---|
| Raw | 22.63 | 2.64 |
| Acid-treated | 32.04 | 2.76 |
| PFA-treated | 39.33 | 2.88 |
| Bleached | 48.63 | 3.92 |
| CNC | 67.16 | 3.72 |

The most conservative XRD phase analysis method for determining cellulose crystallinity was peak deconvolution.[59–61] As illustrated in Fig. S1,† the peak deconvolution technique was used to isolate specific crystalline peaks from the XRD curves to determine the crystallinity of the materials manufactured at various phases using the XRD spectra. Gaussian, Lorentzian, and Voigt functions were typically utilized in deconvolution.[61] All peaks were Gaussian fit in this investigation, and the broad peaks at about 20 and 40° were assigned to the amorphous contribution. In cellulose, an amorphous peak was frequently detected in the $2\theta$ range of 16–20°.[60–62] This study attributed a broad peak around 35° to the crystallinity component to match experimental data. According to Table 1, the RH treated with formic/peroxyformic acid has increased CrI and crystalline domain size.

Acid and PFA treatment disintegrated the amorphous hemicelluloses and lignin, dramatically raising CrI from 22.63% to 39.33%. Bleaching eliminated the remaining amorphous components, producing a maximum CrI of 48.63%. With their removal, a considerable number of crystalline domains can be realigned. The remaining undeveloped areas were sensitive to acid assault and had random orientations. Hydronium ions ($H_3O^+$) can penetrate amorphous regions and encourage the hydrolytic breakage of cellulose's glycosidic linkages, which releases individual crystallites.[61,63–65] A prominent and strong peak was seen in the XRD pattern after acid hydrolysis, supporting the significant 67.16% improvement in crystallinity. The cellulose isolation methods, the hydrolysis process length, the raw materials used in its synthesis, and the data assessment strategy significantly impacted CNC's crystallinity values.[66] The high crystallinity of CNC was crucial in defining the barrier and mechanical (strength, stiffness, and rigidity) qualities of biopolymer composites utilized as fillers in industrial applications.[64,67]

### 3.4. TGA analysis

Thermogravimetric analysis was performed on untreated RH, acid-treated, PFA-treated, bleached, and CNC samples to examine the degradation characteristics at various preparation phases. Fig. 4a depicts the TG curves for sample weight loss at 25 to 800 °C temperatures. Due to the presence of non-cellulosic and cellulosic molecules with different degradation, the thermal decomposition of unprocessed RH was a multi-stage process. The corresponding data for samples in each degradation step are summarized in Table 2. Initial weight loss was


© 2024 The Author(s). Published by the Royal Society of Chemistry

Open Access Article. Published on 09 January 2024. Downloaded on 1/19/2026 7:03:55 PM.
This article is licensed under a Creative Commons Attribution-NonCommercial 3.0 Unported Licence.

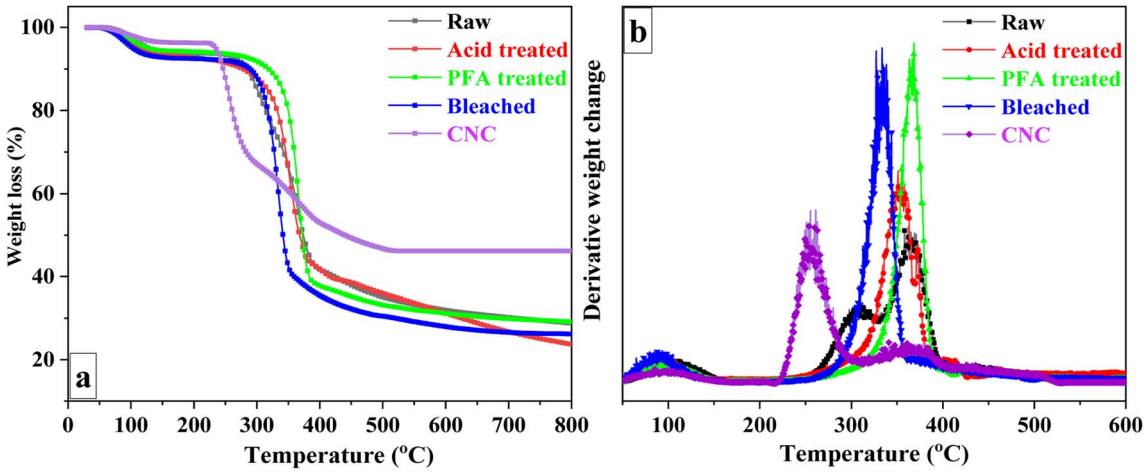


Fig. 4 TGA (a) and DTG (b) curves of RH at different treatment phases.

caused by the evaporation of adsorbed moisture on the surface of RH and intermolecular hydrogen-bonded chemisorbed water between 70 and 120 °C.[68,69] Thermal depolymerization of hemicelluloses and the breaking of glycosidic linkages in cellulose started the next degradation step at 271 °C.[58]

Lignin is more heat stable than cellulose and hemicelluloses due to its aromatic backbone. Thus, lignin, the primary cementing component, was connected to the third breakdown stage. Raw RH's DTG (Fig. 4b) displayed two broad peaks (at 308 °C and 364 °C), represented the various thermal stabilities and fracture temperatures corresponding to the oxygen functional groups in the lignin structure,[70] and a low-intensity peak at 425 °C. The acid-treated sample began to degrade at 310 °C and peaked at 352 °C. The PFA-treated sample, on the other hand, began at a higher temperature and reached its highest point at 366 °C. The increase in degradation start temperature was related to flame-retardant lignin on the surface. The bleached RH DTG curve (Fig. 4b) demonstrated a significant weight loss in the range of 280 and 360 °C, with the maximum degradation peak due to the degradation of cellulose being observed at 334 °C.

In contrast to bleached RH, CNC exhibited a significant difference in decomposition behavior. It was discovered that degradation occurred at a lower temperature than bleached RH. The reduced thermal stability can be attributed to two factors: (1) the substantial surface area of the nanocellulose crystals, which increases the surface area exposed to heat,[67,71,72] and (2) the presence of sulfate groups on the CNC surface, which exert a catalytic influence and decrease the activation energy required for cellulose chain degradation.[73] Furthermore, the crystalline structure of CNC[74] and the flame-retardant properties of sulfate groups[75] may contribute to forming more char residue in bleached RH.

The thermal behaviors of samples when heated between 25 °C and 800 °C are shown by the DTA curve in Fig. 5. The endothermal peak at roughly 100 °C in the raw RH indicated that adsorption moisture was evaporating. In addition, the degradation of RH's hemicellulose, cellulose, and lignin components

Table 2 Onset temperature ($T_{onset}$), weight loss ($W_L$), degradation temperature at max weight loss ($T_{max}$), and char yield for RH at different treatment stages evaluated from TG

| | | Raw | Acid treated | PFA treated | Bleached | CNC |
|---|---|---|---|---|---|---|
| Step I | $T_o$ (°C) | 77 | 70 | 72 | 66 | 70 |
| | $T_{max}$ (°C) | 108 | 98 | 98 | 90 | 98 |
| | $W_L$ (%) | 6.3 | 6.6 | 5.6 | 7.4 | 3.7 |
| Step II | $T_o$ (°C) | 271 | — | — | | 236 |
| | $T_{max}$ (°C) | 308 | — | — | | 255 |
| | $W_L$ (%) | 18.9 | — | — | | 30.3 |
| Step III | $T_o$ (°C) | 348 | 310 | 327 | 310 | 280 |
| | $T_{max}$ (°C) | 364 | 352 | 366 | 334 | 371 |
| | $W_L$ (%) | 33.5 | 49.5 | 56.5 | 59.4 | 13.8 |
| Step IV | $T_o$ (°C) | 413 | 385 | 384 | — | 390 |
| | $T_{max}$ (°C) | 425 | 402 | 430 | — | 428 |
| | $W_L$ (%) | 7.1 | 3.8 | 4.2 | — | 5.8 |
| Char yield (%) at 800 °C | | 28.7 | 23.6 | 29.2 | 26.2 | 46.2 |

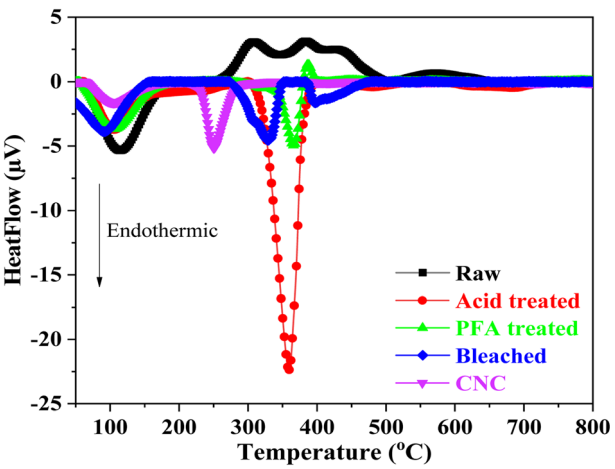


Fig. 5 DTA curves of RH at different stages of treatment.

Open Access Article. Published on 09 January 2024. Downloaded on 1/19/2026 7:03:55 PM. This article is licensed under a Creative Commons Attribution-NonCommercial 3.0 Unported Licence.

was linked to two prominent exothermal peaks that overlapped between 250 °C and 500 °C.

The endothermal peak of the acid and PFA-treated samples' DTA curves below 150 °C suggested that the samples' adsorbed moisture had evaporated, which was in line with the weight loss seen in the TGA analysis. TGA and DTA investigations showed that two samples had less adsorbed water than raw RH. When the hemicellulose components of RH were subjected to HCOOH acid and HCOOH/$H_2O_2$ acid at 80 °C, they disintegrated. The lignin component was flattened and moved toward the surface, suppressing moisture adsorption capacity due to the hydrophobic property of lignin.

Based on the DTA results, it can be concluded that the formic/peroxyformic acid treatment RH underwent endothermal thermal degradation that occurred at higher temperatures than untreated RH. After the PFA treatment, the RH was bleached in a NaOH and $H_2O_2$ solution. The breakdown of $H_2O_2$ into $H^+$ and perhydroxyl ions ($HO_2^-$) was accelerated by the presence of NaOH. These ions attacked the double bonds on the chain and aromatic ring derivatives in lignin, breaking the outer lignin structure and releasing the cellulose component inside the RH.

The DTA analysis of the bleached thermogram revealed an endotherm below 150 °C, which can be ascribed to water loss. A second endothermic transition, which takes place between 280 °C and 360 °C, signifies the fusion of crystallites and reflects the characteristic decomposition of cellulose within this temperature range.[38] DTA investigations also revealed a significant difference in thermal behavior between CNC and bleached RH. A broad endothermic range of 280 °C to 360 °C was observed for the bleached sample. In contrast, the CNC exhibited an abrupt and narrow endotherm beginning at 230 °C with a peak at 250 °C. This was probably due to the replacement of hydroxyl groups by sulfate groups (O–$SO_3H$) during the hydrolysis step. The literature has documented that the sulfate groups found in CNC facilitate direct solid-to-gas phase transitions in nanocellulose crystals.[76,77] This leads to a gradual decomposition process preceding the pyrolysis of the primary cellulose. The crystalline structure and particle size are drastically altered during sulfation, resulting in an earlier fusion initiation in CNC than bleached RH. These findings were relevant to the TGA analysis.

### 3.5. Transmission electron microscopy analysis

TEM observations of the morphology of bleached RH and CNC are depicted in Fig. 6. It validated the data showing that RH-isolated cellulose nanofibrils existed. Long fibrils with widths in the nanometer range (1–10 nm) were portrayed in the photograph. The length-to-diameter or aspect ratio substantially impacts how well nanofibers can reinforce materials. Aspect ratios for most fibers ranged from 120 to 140. This value was relatively high compared to cellulose nanofibrils isolated from other sources, such as wheat straw (90–110)[78] or coconut shell (60).[79] As shown in Fig. 6b, acid treatment successfully hydrolyzed and removed the amorphous region in cellulose nanofibrils, causing a substantial length reduction and hydrolyzed cellulose-generated rod-like structures. CNC, generated from RH, had an aspect ratio of 10.2 ± 6.8, a diameter of 19 ± 3.3 nm, and a length of 195 ± 24 nm. The aspect ratio determines how well nanofibers can act as reinforcement. CNC's more excellent aspect ratio may be employed as a filler for reinforcement within the film to strengthen the biocomposite's mechanical properties.[80] Similar aspect ratios were reported for CNC extracted from grape skin (5–10), rice straw (8.8–10.5),[81] Mengkuang leaves (10–20),[82] raw cotton linter (19),[83] degreasing cotton (12 ± 10), and waste cotton cloth (17 ± 15).[84] Roohani *et al.* isolated a CNC with an average width, length, and aspect ratio of 14.6 nm, 171 nm, and 11–12.[85] According to Chandra *et al.*, cellulose nanofibers made from areca nut husk fibers exhibited a high aspect ratio of 120–150 and a 1–10 nm diameter.[86]

In the current research, the yield of CNC extracted from RH ranged between 28% and 30%, more significant than the yield (12%) of CNC extracted from RH in a previous study.[87] The utilization of various acids and hydrolysis conditions may be the cause of the yield difference. This yield was similar to the CNC obtained from okra fibers (30%) and Mengkuang leaves (28%).[82,88] In contrast, the percentage yield of CNC derived from RH was lower than that of CNC obtained from areca nut fibers

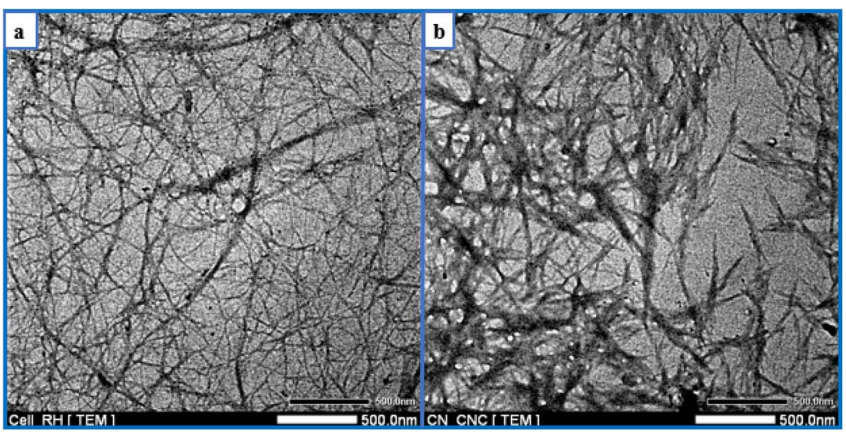


Fig. 6 TEM images of (a) bleached RH and (b) CNC.


© 2024 The Author(s). Published by the Royal Society of Chemistry

Open Access Article. Published on 09 January 2024. Downloaded on 1/19/2026 7:03:55 PM.
This article is licensed under a Creative Commons Attribution-NonCommercial 3.0 Unported Licence.

(35 ± 0.2%)[89] and sugarcane bagasse (66.45%)[90] and higher than that of CNC obtained from barley straw and husk (12%)[91] and old corrugated container fiber (23.98%).[92] The cellulose source and the isolation conditions have the most significant impact on CNC yield. It is possible that the use of mechanical pre-treatment on cellulose, combined with acid hydrolysis under precisely controlled conditions, including acid concentration, hydrolysis time, and temperature, and followed by post-treatment procedures, such as homogenization and ultrasonication, will increase the production yield of CNC.[93]

### 3.6. Raman analysis

Due to its high sensitivity to changes in the hydrogen bonding environment, Raman spectroscopy was used to detect changes in the polymorphic arrangement of cellulose.[94] The Raman spectra obtained from three separate scans carried out on various areas of the CNC sample are shown in Fig. 7a. The resulting band pattern resembles those found in earlier research.[94,95] Bands produced by the vibrations of COC, $CH_2$, CH, and OH groups, as well as the likely vibrations of CH–O and OH–O hydrogen bonds, predominated in this range between 250 and 1600 $cm^{-1}$. The bands that best reflected the molecular surroundings of the methylene (–$CH_2$) and methine (–CH) groups were 1478–1464 $cm^{-1}$, 1376–1337 $cm^{-1}$, 1263–1286 $cm^{-1}$, and 980 $cm^{-1}$. $CH_2$ scissoring (bending) deformations and OH bending deformations at C-6 were principally responsible for bands at 1478 $cm^{-1}$ and 1464 $cm^{-1}$.[96,97] These bands revealed details on cellulose's intramolecular and intermolecular bonds' ultrastructure.[94]

The glycosidic linkage orientation was sensitive between 1200 and 1300 $cm^{-1}$. A weak band at 1286 $cm^{-1}$ and a strong band at 1263 $cm^{-1}$ were discernible in this area (Fig. 7c). While the latter was connected to cellulose II, the former has been seen before in bacterial and wood cellulose I. The $CH_2$ group vibrations were linked to the bands at 980 $cm^{-1}$. C–O–C glycosidic linkage deformations caused the 1121, 1092, and 490 $cm^{-1}$ bands. Ring deformations were apparent between 541 and 1147 $cm^{-1}$ (Fig. 7b and c). The 435 and 421 $cm^{-1}$ bands were connected to CCC and CCO ring vibrations, respectively. Bands at about 435 $cm^{-1}$ were typical of cellulose I, whereas bands at 421 $cm^{-1}$ were unique to cellulose II.[98]

Agarwal proved that bands at about 380 $cm^{-1}$ are related to the cellulose crystallinity index.[95] Bands at 327 $cm^{-1}$ and 580 $cm^{-1}$, respectively, are other skeletal deformations indicative of cellulose I (Fig. 7b). The bending vibration of the methine group at C-1 or the bending vibration of HCC and HCO at C-6 in the pyranose unit were responsible for the broadband between 840 and 880 $cm^{-1}$.[98]

### 3.7. $^{13}$C-NMR analysis

Carbon from cellulose has $^{13}$C NMR signals between 60 and 110 ppm. Fig. 8 depicts the CNC spectrum extracted from RH. The peaks at 72.4 ppm and 73.6 ppm were cellulose carbons C-2 and C-3, respectively. The peak at 75.5 ppm was cellulose carbon C-5. The peak represented crystalline cellulose carbon C-4 at 89.3 ppm, while the peak represented crystalline cellulose carbon C-1 at 105.5 ppm.[99]

The C-6 peak suggested crystalline cellulose at 65.7 ppm.[100] The NMR spectra showed that most hemicellulose and lignin were removed after chemical processes (acid treatment, PFA treatment, bleaching, and hydrolysis). Eliminating C-1 from the hemicellulose's (1-4)-D-Xylp-2-*O*-(4-OMe-dGlcpA) units cause the 102 ppm peak to be absent.[101] Furthermore, the absence of representative peaks of hemicellulose and lignin at 21, 56, or 173 ppm[102] suggested that the chemical treatments removed the carbons in lignin's methyl, methoxyl, and carboxylic groups.

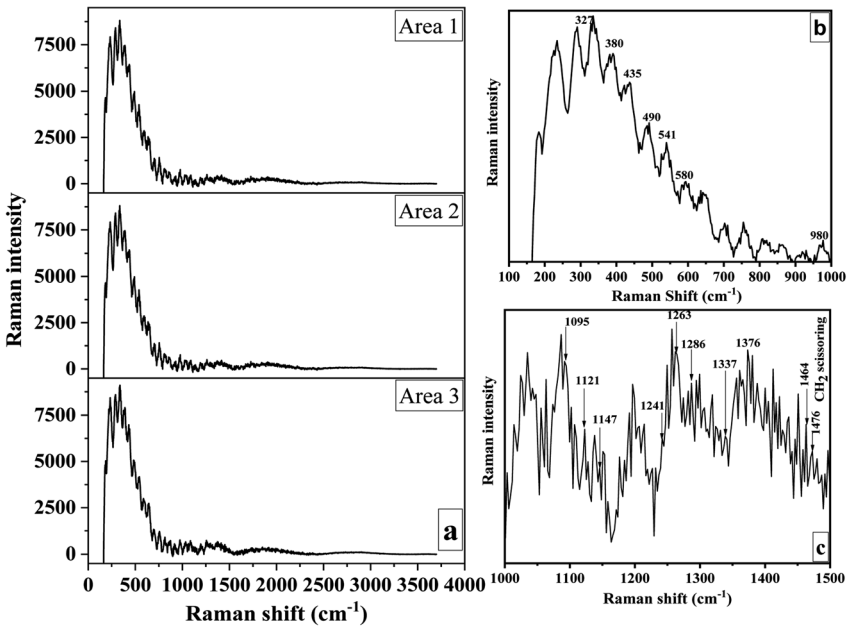


Fig. 7 Raman spectra of three separate scans of distinct CNC regions (a) and within specified band regions (b and c).

Open Access Article. Published on 09 January 2024. Downloaded on 1/19/2026 7:03:55 PM.
This article is licensed under a Creative Commons Attribution-NonCommercial 3.0 Unported Licence.

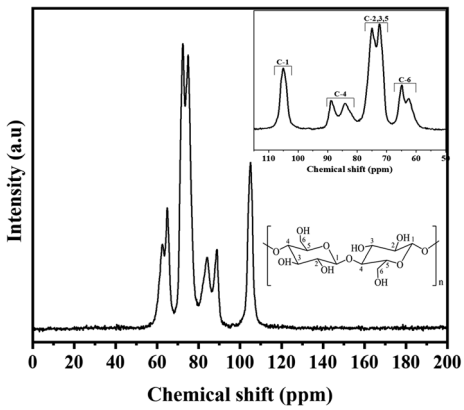


Fig. 8 $^{13}C$ NMR spectra of CNC.

In conclusion, the spectra of CNC elucidated that each peak originated from six carbon atoms within the cellulose structure.

## 4. Conclusion

Using a formic/peroxyformic procedure, we successfully extracted cellulose from rice husk (RH). The technique above successfully eliminated non-cellulose components while also inducing swelling and migration of lignin toward the RH's surface, minimizing the requirement for recurrent bleaching and shortening the bleaching process. To create cellulose nanocrystals (CNC), 64% sulfuric acid was used to hydrolyze the cellulose. With the CNC, cellulose's crystallinity rose from 22.63% with the raw RH to 67.16%. The leading cause was the isolation and hydrolysis processes, which eliminated amorphous components like hemicellulose, lignin, pectin, and the fiber structure's loosely organized underdeveloped cellulose region. After $H_2SO_4$ hydrolysis, a rod-like CNC was produced. With an aspect ratio of 10.2 $\pm$ 6.8, CNC had a diameter and length of 19 $\pm$ 3.3 nm and 195 $\pm$ 24 nm. According to the research, CNC offers excellent promise for using nanocomposite materials as a reinforcing phase.

## Data availability

Data will be made available on request.

## Author contributions

An Nang Vu: conceptualization, investigation, writing – original draft preparation. Long Hoang Nguyen: formal analysis. Ha-Chi V. Tran: formal analysis. Kimio Yoshimura: resources. Tap Duy Tran: investigation. Hieu Van Le: writing – review & editing. Ngoc-Uyen T. Nguyen: conceptualization, validation, supervision.

## Conflicts of Interest

The authors report no declarations of interest.

## Acknowledgements

This research is funded by Vietnam National University Ho Chi Minh City (VNU-HCM) under grant number VL2020-18-05. The authors are grateful for this financial support.

## References

1 S. S. Hassan, G. A. Williams and A. K. Jaiswal, Emerging technologies for the pretreatment of lignocellulosic biomass, *Bioresour. Technol.*, 2018, **262**, 310–318.
2 I. S. Makarov, L. K. Golova, G. N. Bondarenko, T. S. Anokhina, E. S. Dmitrieva, I. S. Levin, *et al.*, Structure, Morphology, and Permeability of Cellulose Films, *Membranes*, 2022, **12**(3), 297–309.
3 K. V. Neenu, C. D. Midhun Dominic, P. M. S. Begum, J. Parameswaranpillai, B. P. Kanoth, D. A. David, *et al.*, Effect of oxalic acid and sulphuric acid hydrolysis on the preparation and properties of pineapple pomace derived cellulose nanofibers and nanopapers, *Int. J. Biol. Macromol.*, 2022, **209**, 1745–1759.
4 P. Bagde and V. Nadanathangam, Mechanical, antibacterial and biodegradable properties of starch film containing bacteriocin immobilized crystalline nanocellulose, *Carbohydr. Polym.*, 2019, **222**, 115021.
5 C. Amara, A. El Mahdi, R. Medimagh and K. Khwaldia, Nanocellulose-based composites for packaging applications, *Curr. Opin. Green Sustainable Chem.*, 2021, **31**, 100512.
6 K. Daicho, K. Kobayashi, S. Fujisawa and T. Saito, Crystallinity-Independent yet Modification-Dependent True Density of Nanocellulose, *Biomacromolecules*, 2020, **21**(2), 939–945.
7 M. Osorio, P. Fernández-Morales, P. Gañán, R. Zuluaga, H. Kerguelen, I. Ortiz, *et al.*, Development of novel three-dimensional scaffolds based on bacterial nanocellulose for tissue engineering and regenerative medicine: Effect of processing methods, pore size, and surface area, *J. Biomed. Mater. Res., Part A*, 2019, **107**(2), 348–359.
8 L. K. Kian, N. Saba, M. Jawaid and M. T. H. Sultan, A review on processing techniques of bast fibers nanocellulose and its polylactic acid (PLA) nanocomposites, *Int. J. Biol. Macromol.*, 2019, **121**, 1314–1328.
9 S. S. Ahankari, A. R. Subhedar, S. S. Bhadauria and A. Dufresne, Nanocellulose in food packaging: A review, *Carbohydr. Polym.*, 2021, **255**, 117479.
10 L. Cao, J. Huang, J. Fan, Z. Gong, C. Xu and Y. Chen, Nanocellulose-A Sustainable and Efficient Nanofiller for Rubber Nanocomposites: From Reinforcement to Smart Soft Materials, *Polym. Rev.*, 2022, **62**(3), 549–584.
11 A. Hachaichi, B. Kouini, L. K. Kian, M. Asim, H. Fouad, M. Jawaid, *et al.*, Nanocrystalline Cellulose from Microcrystalline Cellulose of Date Palm Fibers as a Promising Candidate for Bio-Nanocomposites: Isolation and Characterization, *Materials*, 2021, **14**(18), 5313.
12 N. Raghav, M. R. Sharma and J. F. Kennedy, Nanocellulose: A mini-review on types and use in drug delivery systems, *Carbohydr. Polym. Technol. Appl.*, 2021, **2**, 100031.


© 2024 The Author(s). Published by the Royal Society of Chemistry

Open Access Article. Published on 09 January 2024. Downloaded on 1/19/2026 7:03:55 PM. This article is licensed under a Creative Commons Attribution-NonCommercial 3.0 Unported Licence.

13 J. A. Kelly, A. M. Shukaliak, C. C. Y. Cheung, K. E. Shopsowitz, W. Y. Hamad and M. J. MacLachlan, Responsive Photonic Hydrogels Based on Nanocrystalline Cellulose, *Angew. Chem., Int. Ed.*, 2013, **52**(34), 8912–8916.
14 F. H. Bagis and Setiadi, Nanocellulose filament fabrication from Sugarcane Bagasse through wet spinning method, *AIP Conf. Proc.*, 2020, **2255**(1), 040005.
15 J. Nemoto, T. Saito and A. Isogai, Simple Freeze-Drying Procedure for Producing Nanocellulose Aerogel-Containing, High-Performance Air Filters, *ACS Appl. Mater. Interfaces*, 2015, **7**(35), 19809–19815.
16 Y. Qin, J. Mo, Y. Liu, S. Zhang, J. Wang, Q. Fu, *et al.*, Stretchable Triboelectric Self-Powered Sweat Sensor Fabricated from Self-Healing Nanocellulose Hydrogels, *Adv. Funct. Mater.*, 2022, **32**(27), 2201846.
17 T. Bayer, B. V. Cunning, R. Selyanchyn, M. Nishihara, S. Fujikawa, K. Sasaki, *et al.*, High Temperature Proton Conduction in Nanocellulose Membranes: Paper Fuel Cells, *Chem. Mater.*, 2016, **28**(13), 4805–4814.
18 V. C.-F. Li, C. K. Dunn, Z. Zhang, Y. Deng and H. J. Qi, Direct Ink Write (DIW) 3D Printed Cellulose Nanocrystal Aerogel Structures, *Sci. Rep.*, 2017, **7**(1), 8018.
19 P. Moharrami and E. Motamedi, Application of cellulose nanocrystals prepared from agricultural wastes for synthesis of starch-based hydrogel nanocomposites: Efficient and selective nanoadsorbent for removal of cationic dyes from water, *Bioresour. Technol.*, 2020, **313**, 123661.
20 S. Li and G. Chen, Agricultural waste-derived superabsorbent hydrogels: Preparation, performance, and socioeconomic impacts, *J. Cleaner Prod.*, 2020, **251**, 119669.
21 C. Sun, J. Ni, C. Zhao, J. Du, C. Zhou, S. Wang, *et al.*, Preparation of a cellulosic adsorbent by functionalization with pyridone diacid for removal of Pb(II) and Co(II) from aqueous solutions, *Cellulose*, 2017, **24**(12), 5615–5624.
22 S. A. A. K. M. Hamed and M. L. Hassan, A new mixture of hydroxypropyl cellulose and nanocellulose for wood consolidation, *J. Cult. Herit.*, 2019, **35**, 140–144.
23 Y. Liu, Q. Fu, J. Mo, Y. Lu, C. Cai, B. Luo, *et al.*, Chemically tailored molecular surface modification of cellulose nanofibrils for manipulating the charge density of triboelectric nanogenerators, *Nano Energy*, 2021, **89**, 106369.
24 H. Du, M. Parit, M. Wu, X. Che, Y. Wang, M. Zhang, *et al.*, Sustainable valorization of paper mill sludge into cellulose nanofibrils and cellulose nanopaper, *J. Hazard. Mater.*, 2020, **400**, 123106.
25 V. K. Thakur, A. S. Singha and M. K. Thakur, Natural Cellulosic Polymers as Potential Reinforcement in Composites: Physicochemical and Mechanical Studies, *Adv. Polym. Technol.*, 2013, **32**(S1), E427.
26 Y.-H. Feng, T.-Y. Cheng, W.-G. Yang, P.-T. Ma, H.-Z. He, X.-C. Yin, *et al.*, Characteristics and environmentally friendly extraction of cellulose nanofibrils from sugarcane bagasse, *Ind. Crops Prod.*, 2018, **111**, 285–291.
27 D. Magalhães do Nascimento, J. Almeida, S. Vale, R. Leitão, C. Muniz and M. Figueirêdo, A comprehensive approach for obtaining cellulose nanocrystal from coconut fiber. Part I: Proposition of technological pathways, *Ind. Crops Prod.*, 2016, **93**, 66–75.
28 P. Lu and Y.-L. Hsieh, Preparation and characterization of cellulose nanocrystals from rice straw, *Carbohydr. Polym.*, 2012, **87**(1), 564–573.
29 S. Mueller, C. Weder and E. J. Foster, Isolation of cellulose nanocrystals from pseudostems of banana plants, *RSC Adv.*, 2014, **4**(2), 907–915.
30 N. H. A. Rahman, N. A. Ibrahim, B. W. Chieng and N. A. Rahman, Extraction and Characterization of Cellulose Nanocrystals from Tea Leaves Waste Fiber, *Polymers*, 2017, **9**(11), 588–598.
31 S. Rungrodnimitchai, W. Phokhanusai and N. Sungkhaho, Preparation of silica gel from rice husk ash using microwave heating, *J. Met., Mater. Miner.*, 2017, **19**(2), 45–50.
32 N. Yuzer, Z. Cinar, F. Akoz, H. Biricik, Y. Yalcin Gurkan, N. Kabay, *et al.*, Influence of raw rice husk addition on structure and properties of concrete, *Constr. Build. Mater.*, 2013, **44**, 54–62.
33 C. N. H. Thuc and H. H. Thuc, Synthesis of silica nanoparticles from Vietnamese rice husk by sol–gel method, *Nanoscale Res. Lett.*, 2013, **8**(1), 58.
34 M. Jackson, The alkali treatment of straws, *Anim. Feed Sci. Technol.*, 1977, **2**(2), 105–130.
35 E. S. Abdel-Halim, Simple and economic bleaching process for cotton fabric, *Carbohydr. Polym.*, 2012, **88**(4), 1233–1238.
36 J. Chandra, N. George and S. K. Narayanankutty, Isolation and characterization of cellulose nanofibrils from arecanut husk fibre, *Carbohydr. Polym.*, 2016, **142**, 158–166.
37 Y. W. Chen, H. V. Lee, J. C. Juan and S.-M. Phang, Production of new cellulose nanomaterial from red algae marine biomass Gelidium elegans, *Carbohydr. Polym.*, 2016, **151**, 1210–1219.
38 S. M. L. Rosa, N. Rehman, M. I. G. de Miranda, S. M. B. Nachtigall and C. I. D. Bica, Chlorine-free extraction of cellulose from rice husk and whisker isolation, *Carbohydr. Polym.*, 2012, **87**(2), 1131–1138.
39 N. E. Fitriana, A. Suwanto, T. H. Jatmiko, S. Mursiti and D. J. Prasetyo, Cellulose extraction from sugar palm (Arenga pinnata) fibre by alkaline and peroxide treatments, *IOP Conf. Ser. Earth Environ. Sci.*, 2020, **462**(1), 012053.
40 I. W. Arnata, F. Fahma, N. Richana and T. C. Sunarti, Cellulose Production from Sago Frond with Alkaline Delignification and Bleaching on Various Types of Bleach Agents, *Orient. J. Chem.*, 2019, **35**, 8–19.
41 R. G. Candido and A. R. Gonçalves, Evaluation of two different applications for cellulose isolated from sugarcane bagasse in a biorefinery concept, *Ind. Crops Prod.*, 2019, **142**, 111616.
42 X. Liu, Y. Li, C. M. Ewulonu, J. Ralph, F. Xu, Q. Zhang, *et al.*, Mild Alkaline Pretreatment for Isolation of Native-Like Lignin and Lignin-Containing Cellulose Nanofibers (LCNF) from Crop Waste, *ACS Sustain. Chem. Eng.*, 2019, **7**(16), 14135–14142.

Open Access Article. Published on 09 January 2024. Downloaded on 1/19/2026 7:03:55 PM. This article is licensed under a Creative Commons Attribution-NonCommercial 3.0 Unported Licence.

43 H. Ji, Z. Xiang, H. Qi, T. Han, A. Pranovich and T. Song, Strategy towards one-step preparation of carboxylic cellulose nanocrystals and nanofibrils with high yield, carboxylation and highly stable dispersibility using innocuous citric acid, *Green Chem.*, 2019, **21**(8), 1956–1964.
44 C. Huang, W. Lin, C. Lai, X. Li, Y. Jin and Q. Yong, Coupling the post-extraction process to remove residual lignin and alter the recalcitrant structures for improving the enzymatic digestibility of acid-pretreated bamboo residues, *Bioresour. Technol.*, 2019, **285**, 121355.
45 B. Li, W. Xu, D. Kronlund, A. Määttänen, J. Liu, J.-H. Smått, *et al.*, Cellulose nanocrystals prepared via formic acid hydrolysis followed by TEMPO-mediated oxidation, *Carbohydr. Polym.*, 2015, **133**, 605–612.
46 M. S. Islam, N. Kao, S. N. Bhattacharya, R. Gupta and P. K. Bhattacharjee, Effect of low pressure alkaline delignification process on the production of nanocrystalline cellulose from rice husk, *J. Taiwan Inst. Chem. Eng.*, 2017, **80**, 820–834.
47 R. M. Dos Santos, W. P. F. Neto, H. A. Silvério, D. F. Martins, N. O. Dantas and D. Pasquini, Cellulose nanocrystals from pineapple leaf, a new approach for the reuse of this agro-waste, *Ind. Crops Prod.*, 2013, **50**, 707–714.
48 A. A. Oun and J.-W. Rhim, Preparation and characterization of sodium carboxymethyl cellulose/cotton linter cellulose nanofibril composite films, *Carbohydr. Polym.*, 2015, **127**, 101–109.
49 F. Jiang and Y.-L. Hsieh, Cellulose nanocrystal isolation from tomato peels and assembled nanofibers, *Carbohydr. Polym.*, 2015, **122**, 60–68.
50 E. H. Qua, P. R. Hornsby, H. S. S. Sharma and G. Lyons, Preparation and characterisation of cellulose nanofibres, *J. Mater. Sci.*, 2011, **46**(18), 6029–6045.
51 J. Lamaming, R. Hashim, C. P. Leh, O. Sulaiman, T. Sugimoto and M. Nasir, Isolation and characterization of cellulose nanocrystals from parenchyma and vascular bundle of oil palm trunk (Elaeis guineensis), *Carbohydr. Polym.*, 2015, **134**, 534–540.
52 J. Li, S. Zhang, B. Gao, A. Yang, Z. Wang, Y. Xia, *et al.*, Characteristics and deoxy-liquefaction of cellulose extracted from cotton stalk, *Fuel*, 2016, **166**, 196–202.
53 G. Mondragon, S. Fernandes, A. Retegi, C. Peña, I. Algar, A. Eceiza, *et al.*, A common strategy to extracting cellulose nanoentities from different plants, *Ind. Crops Prod.*, 2014, **55**, 140–148.
54 E. Robles, I. Urruzola, J. Labidi and L. Serrano, Surface-modified nano-cellulose as reinforcement in poly(lactic acid) to conform new composites, *Ind. Crops Prod.*, 2015, **71**, 44–53.
55 Q. Lu, W. Lin, L. Tang, S. Wang, X. Chen and B. Huang, A mechanochemical approach to manufacturing bamboo cellulose nanocrystals, *J. Mater. Sci.*, 2015, **50**(2), 611–619.
56 Z. Wang, Z. Yao, J. Zhou, M. He, Q. Jiang, S. Li, *et al.*, Isolation and characterization of cellulose nanocrystals from pueraria root residue, *Int. J. Biol. Macromol.*, 2019, **129**, 1081–1089.
57 Y. Nishiyama, Structure and properties of the cellulose microfibril, *J. Wood Sci.*, 2009, **55**(4), 241–249.
58 C. J. Chirayil, J. Joy, L. Mathew, M. Mozetic, J. Koetz and S. Thomas, Isolation and characterization of cellulose nanofibrils from Helicteres isora plant, *Ind. Crops Prod.*, 2014, **59**, 27–34.
59 C. J. Garvey, I. H. Parker and G. P. Simon, On the Interpretation of X-Ray Diffraction Powder Patterns in Terms of the Nanostructure of Cellulose I Fibres, *Macromol. Chem. Phys.*, 2005, **206**(15), 1568–1575.
60 L. Xing, J. Gu, W. Zhang, D. Tu and C. Hu, Cellulose I and II nanocrystals produced by sulfuric acid hydrolysis of Tetra pak cellulose I, *Carbohydr. Polym.*, 2018, **192**, 184–192.
61 S. Park, J. O. Baker, M. E. Himmel, P. A. Parilla and D. K. Johnson, Cellulose crystallinity index: measurement techniques and their impact on interpreting cellulase performance, *Biotechnol. Biofuels*, 2010, **3**, 1–10.
62 A. D. French and M. Santiago Cintrón, Cellulose polymorphy, crystallite size, and the Segal Crystallinity Index, *Cellulose*, 2013, **20**(1), 583–588.
63 M. M. de Souza Lima and R. Borsali, Rodlike Cellulose Microcrystals: Structure, Properties, and Applications, *Macromol. Rapid Commun.*, 2004, **25**(7), 771–787.
64 S. Collazo-Bigliardi, R. Ortega-Toro and A. Chiralt Boix, Isolation and characterisation of microcrystalline cellulose and cellulose nanocrystals from coffee husk and comparative study with rice husk, *Carbohydr. Polym.*, 2018, **191**, 205–215.
65 H. Doh, M. H. Lee and W. S. Whiteside, Physicochemical characteristics of cellulose nanocrystals isolated from seaweed biomass, *Food Hydrocolloids*, 2020, **102**, 105542.
66 H. Vieyra, U. Figueroa-López, A. Guevara-Morales, B. Vergara-Porras, E. San Martín-Martínez and M. Á. Aguilar-Mendez, Optimized Monitoring of Production of Cellulose Nanowhiskers from *Opuntia ficus-indica* (Nopal Cactus), *Int. J. Polym. Sci.*, 2015, **2015**, 871345.
67 S. Naduparambath, T. V. Jinitha, V. Shaniba, M. P. Sreejith, A. K. Balan and E. Purushothaman, Isolation and characterisation of cellulose nanocrystals from sago seed shells, *Carbohydr. Polym.*, 2018, **180**, 13–20.
68 H. Dai, S. Ou, Y. Huang and H. Huang, Utilization of pineapple peel for production of nanocellulose and film application, *Cellulose*, 2018, **25**(3), 1743–1756.
69 O. Prakash, M. Naik, R. Katiyar, S. Naik, D. Kumar, D. Maji, *et al.*, Novel process for isolation of major bio-polymers from Mentha arvensis distilled biomass and saccharification of the isolated cellulose to glucose, *Ind. Crops Prod.*, 2018, **119**, 1–8.
70 M. Brebu and C. Vasile, Thermal degradation of lignin—a review, *Cellul. Chem. Technol.*, 2010, **44**(9), 353.
71 F. Hemmati, S. M. Jafari, M. Kashaninejad and M. Barani Motlagh, Synthesis and characterization of cellulose nanocrystals derived from walnut shell agricultural residues, *Int. J. Biol. Macromol.*, 2018, **120**, 1216–1224.
72 A. Y. Melikoğlu, S. E. Bilek and S. Cesur, Optimum alkaline treatment parameters for the extraction of cellulose and

 © 2024 The Author(s). Published by the Royal Society of Chemistry

Open Access Article. Published on 09 January 2024. Downloaded on 1/19/2026 7:03:55 PM. This article is licensed under a Creative Commons Attribution-NonCommercial 3.0 Unported Licence.

production of cellulose nanocrystals from apple pomace, *Carbohydr. Polym.*, 2019, **215**, 330–337.
73 E. de Morais Teixeira, A. C. Corrêa, A. Manzoli, F. de Lima Leite, C. R. de Oliveira and L. H. C. Mattoso, Cellulose nanofibers from white and naturally colored cotton fibers, *Cellulose*, 2010, **17**(3), 595–606.
74 J. George, K. V. Ramana, A. S. Bawa and Siddaramaiah, Bacterial cellulose nanocrystals exhibiting high thermal stability and their polymer nanocomposites, *Int. J. Biol. Macromol.*, 2011, **48**(1), 50–57.
75 M. Roman and W. T. Winter, Effect of Sulfate Groups from Sulfuric Acid Hydrolysis on the Thermal Degradation Behavior of Bacterial Cellulose, *Biomacromolecules*, 2004, **5**(5), 1671–1677.
76 P. Lu and Y.-L. Hsieh, Preparation and properties of cellulose nanocrystals: rods, spheres, and network, *Carbohydr. Polym.*, 2010, **82**(2), 329–336.
77 N. Wang, E. Ding and R. Cheng, Thermal degradation behaviors of spherical cellulose nanocrystals with sulfate groups, *Polymer*, 2007, **48**(12), 3486–3493.
78 A. Alemdar and M. Sain, Isolation and characterization of nanofibers from agricultural residues – Wheat straw and soy hulls, *Bioresour. Technol.*, 2008, **99**(6), 1664–1671.
79 M. F. Rosa, E. S. Medeiros, J. A. Malmonge, K. S. Gregorski, D. F. Wood, L. H. C. Mattoso, *et al.*, Cellulose nanowhiskers from coconut husk fibers: Effect of preparation conditions on their thermal and morphological behavior, *Carbohydr. Polym.*, 2010, **81**(1), 83–92.
80 M. El Achaby, N. El Miri, A. Aboulkas, M. Zahouily, E. Bilal, A. Barakat, *et al.*, Processing and properties of eco-friendly bio-nanocomposite films filled with cellulose nanocrystals from sugarcane bagasse, *Int. J. Biol. Macromol.*, 2017, **96**, 340–352.
81 Y.-L. Hsieh, Cellulose nanocrystals and self-assembled nanostructures from cotton, rice straw and grape skin: a source perspective, *J. Mater. Sci.*, 2013, **48**(22), 7837–7846.
82 R. M. Sheltami, I. Abdullah, I. Ahmad, A. Dufresne and H. Kargarzadeh, Extraction of cellulose nanocrystals from mengkuang leaves (Pandanus tectorius), *Carbohydr. Polym.*, 2012, **88**(2), 772–779.
83 J. P. S. Morais, M. d. F. Rosa, M. d. s. M. de Souza Filho, L. D. Nascimento, D. M. do Nascimento and A. R. Cassales, Extraction and characterization of nanocellulose structures from raw cotton linter, *Carbohydr. Polym.*, 2013, **91**(1), 229–235.
84 Z. Wang, Z. Yao, J. Zhou and Y. Zhang, Reuse of waste cotton cloth for the extraction of cellulose nanocrystals, *Carbohydr. Polym.*, 2017, **157**, 945–952.
85 M. Roohani, Y. Habibi, N. M. Belgacem, G. Ebrahim, A. N. Karimi and A. Dufresne, Cellulose whiskers reinforced polyvinyl alcohol copolymers nanocomposites, *Eur. Polym. J.*, 2008, **44**(8), 2489–2498.
86 C. S. Chandra, N. George and S. K. Narayanankutty, Isolation and characterization of cellulose nanofibrils from arecanut husk fibre, *Carbohydr. Polym.*, 2016, **142**, 158–166.
87 D. Barana, A. Salanti, M. Orlandi, D. S. Ali and L. Zoia, Biorefinery process for the simultaneous recovery of lignin, hemicelluloses, cellulose nanocrystals and silica from rice husk and Arundo donax, *Ind. Crops Prod.*, 2016, **86**, 31–39.
88 E. Fortunati, D. Puglia, M. Monti, C. Santulli, M. Maniruzzaman and J. M. Kenny, Cellulose nanocrystals extracted from okra fibers in PVA nanocomposites, *J. Appl. Polym. Sci.*, 2013, **128**(5), 3220–3230.
89 S. Ramesh and P. Radhakrishnan, Areca nut fiber nano crystals, clay nano particles and PVA blended bionanocomposite material for active packaging of food, *Appl. Nanosci.*, 2022, **12**(3), 295–307.
90 C. Verma, M. Chhajed, P. Gupta, S. Roy and P. K. Maji, Isolation of cellulose nanocrystals from different waste bio-mass collating their liquid crystal ordering with morphological exploration, *Int. J. Biol. Macromol.*, 2021, **175**, 242–253.
91 E. Fortunati, P. Benincasa, G. M. Balestra, F. Luzi, A. Mazzaglia, D. Del Buono, *et al.*, Revalorization of barley straw and husk as precursors for cellulose nanocrystals extraction and their effect on PVA_CH nanocomposites, *Ind. Crops Prod.*, 2016, **92**, 201–217.
92 Y. Tang, X. Shen, J. Zhang, D. Guo, F. Kong and N. Zhang, Extraction of cellulose nano-crystals from old corrugated container fiber using phosphoric acid and enzymatic hydrolysis followed by sonication, *Carbohydr. Polym.*, 2015, **125**, 360–366.
93 Y. Li, H. Zhu, M. Xu, Z. Zhuang, M. Xu and H. Dai, High Yield Preparation Method of Thermally Stable Cellulose Nanofibers, *BioResources*, 2014, **9**(2), 1986–1997.
94 Q. Li and S. Renneckar, Supramolecular Structure Characterization of Molecularly Thin Cellulose I Nanoparticles, *Biomacromolecules*, 2011, **12**(3), 650–659.
95 U. P. Agarwal, 1064 nm FT-Raman spectroscopy for investigations of plant cell walls and other biomass materials, *Front. Plant Sci.*, 2014, **5**, 490.
96 R. H. Atalla and D. L. VanderHart, Studies on the structure of cellulose using Raman spectroscopy and solid state 13C NMR, *Cellulose and Wood: Chemistry and Technology, Proceedings of the Tenth Cellulose Conference*, ed. C. Schuerch, John Wiley and Sons, New York, 1989.
97 J. H. Wiley and R. H. Atalla, Band assignments in the raman spectra of celluloses, *Carbohydr. Res.*, 1987, **160**, 113–129.
98 K. Schenzel and S. Fischer, NIR FT Raman spectroscopy-a rapid analytical tool for detecting the transformation of cellulose polymorphs, *Cellulose*, 2001, **8**, 49–57.
99 H. Wikberg and S. Liisa Maunu, Characterisation of thermally modified hard- and softwoods by 13C CPMAS NMR, *Carbohydr. Polym.*, 2004, **58**(4), 461–466.
100 C. Vivian Abiaziem, A. Bassey Williams, A. Ibijoke Inegbenebor, C. Theresa Onwordi, C. Osereme Ehi-Eromosele and L. Felicia Petrik, Preparation and Characterisation of Cellulose Nanocrystal from Sugarcane Peels by XRD, SEM and CP/MAS 13C NMR, *J. Phys.: Conf. Ser.*, 2019, **1299**(1), 012123.

© 2024 The Author(s). Published by the Royal Society of Chemistry

Open Access Article. Published on 09 January 2024. Downloaded on 1/19/2026 7:03:55 PM.
This article is licensed under a Creative Commons Attribution-NonCommercial 3.0 Unported Licence.

101 J.-L. Wen, L.-P. Xiao, Y.-C. Sun, S.-N. Sun, F. Xu, R.-C. Sun, *et al.*, Comparative study of alkali-soluble hemicelluloses isolated from bamboo (Bambusa rigida), *Carbohydr. Res.*, 2011, **346**(1), 111–120.

102 A. Idström, S. Schantz, J. Sundberg, B. F. Chmelka, P. Gatenholm and L. Nordstierna, 13C NMR assignments of regenerated cellulose from solid-state 2D NMR spectroscopy, *Carbohydr. Polym.*, 2016, **151**, 480–487.


© 2024 The Author(s). Published by the Royal Society of Chemistry